

Supporting Information

Radiation Damage During *In-Situ* Electron Microscopy of DNA-Mediated Nanoparticle Assemblies in Solution

Peter Sutter,^{1,*} Bo Zhang² and Eli Sutter²

¹Department of Electrical & Computer Engineering, ²Department of Mechanical & Materials Engineering, University of Nebraska-Lincoln, Lincoln NE 68588 (USA)

Supporting Figures

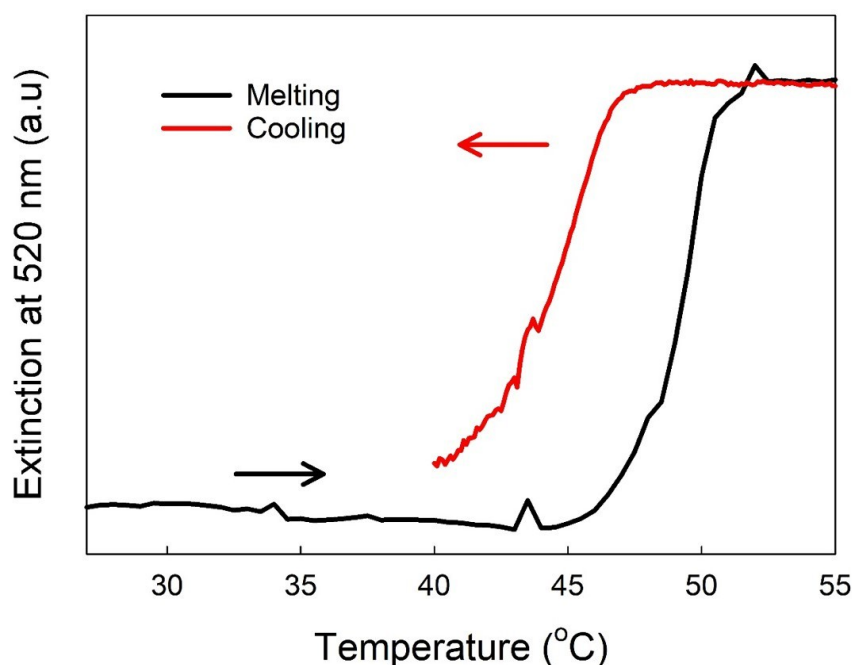


Figure S1. Melting and crystallization of DNA-linked nanoparticle superlattices. UV-VIS spectroscopy of the extinction at a fixed wavelength of 520 nm during slow heating (black line) and cooling (red line) of suspensions of DNA-Au nanoparticle (NP) conjugates with functional linker DNA (as shown in Fig. 1 (a) of the main text) in aqueous solutions of 10 mM phosphate buffer and 0.5 M NaCl. Note the sharp melting transition upon heating at $T \sim 49^\circ\text{C}$, associated by an increase in extinction at 520 nm due to re-dispersion of the previously aggregated NPs. Upon slow cooling, the DNA-Au NP conjugates self-assemble into supracrystals as shown in Figs. 1 (b)-(c) of the main text.

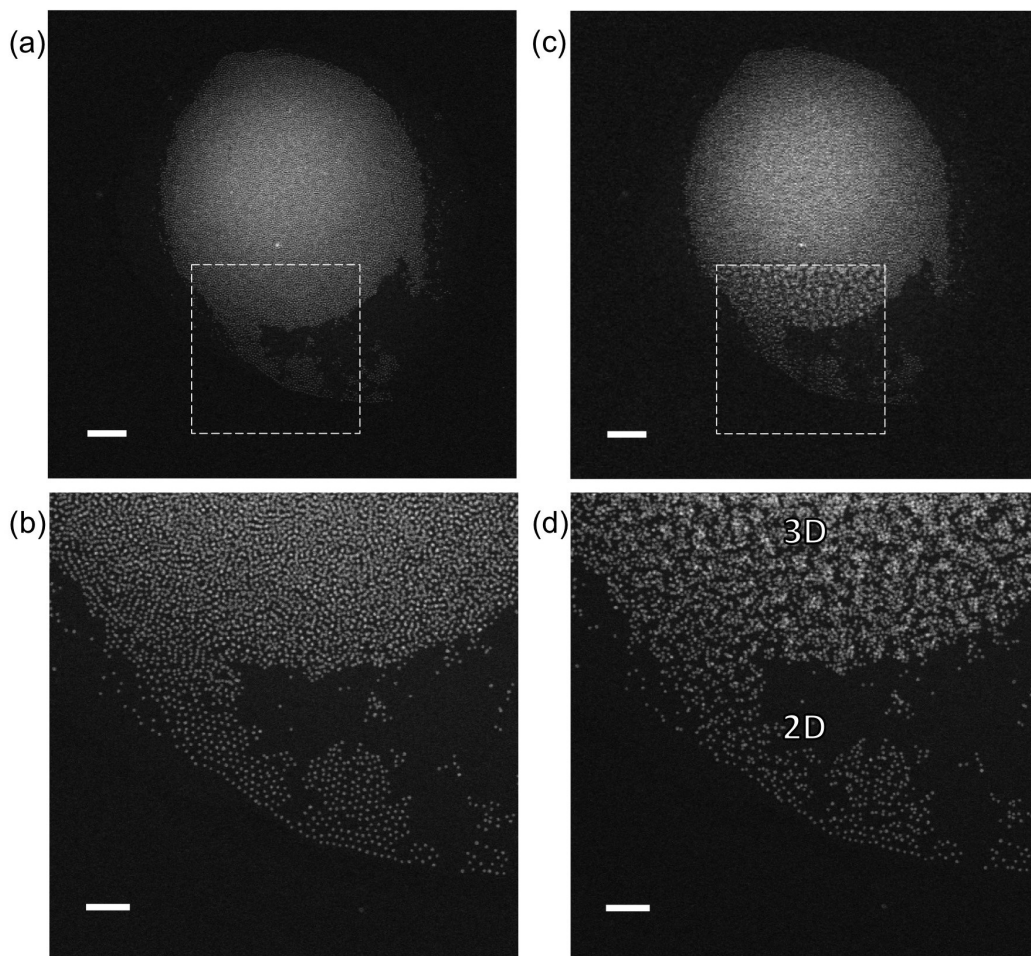


Figure S2. Radiation damage in 3D DNA-mediated Au nanoparticle (NP) assemblies. (a) Liquid-cell scanning transmission electron microscopy (STEM) of the DNA-linked 3D Au NP assembly shown in Fig. 2 (a) (main text), imaged with minimal electron dose. Scale bar: 500 nm. (b) Higher magnification view of the area outlined by a dashed square in (a). Scale bar: 200 nm. (c) Same cluster after continuous STEM imaging of the outlined area at 200 keV electron energy. Scale bar: 500 nm. (d) Higher magnification view of the scanned area, showing significant electron beam-induced displacements in the position of the Au NPs both in the 3D part of the cluster and in the 2D assembly near the periphery. For electron dose information, see Table S1.

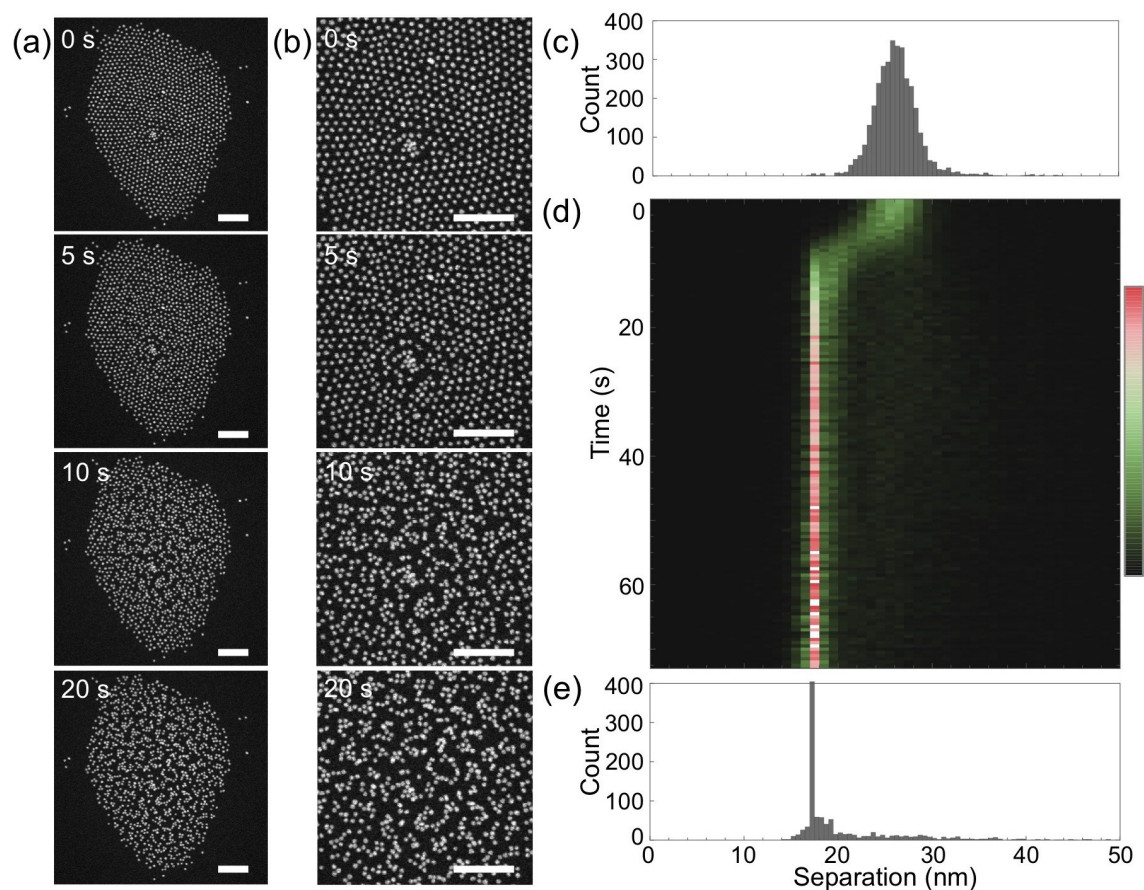


Figure S3. Evolution of 2D assemblies of ‘dummy’ linker terminated particles. (a) Time-lapse sequence of STEM images (primary energy: 200 keV), showing a 2D assembly in the initial state (minimal electron dose), and after 5 s, 10 s, and 20 s of low-dose *in-situ* STEM imaging in solution ($t_{\text{img}} = 1.05$ s). Scale bars: 200 nm. (b) Higher magnification of the center regions of the image series shown in (a). (c) Histogram of center-to-center particle separation at $t = 0$. (d) Density plot of the time dependent particle separation during continuous low-dose STEM imaging for a total duration of 73 sec. Note the rapid contraction in the interparticle spacing during the initial 10 s of electron exposure. (e) Final histogram of center-to-center particle separation after 73 s exposure to 200 keV electrons in STEM. For electron dose information, see Table S1.

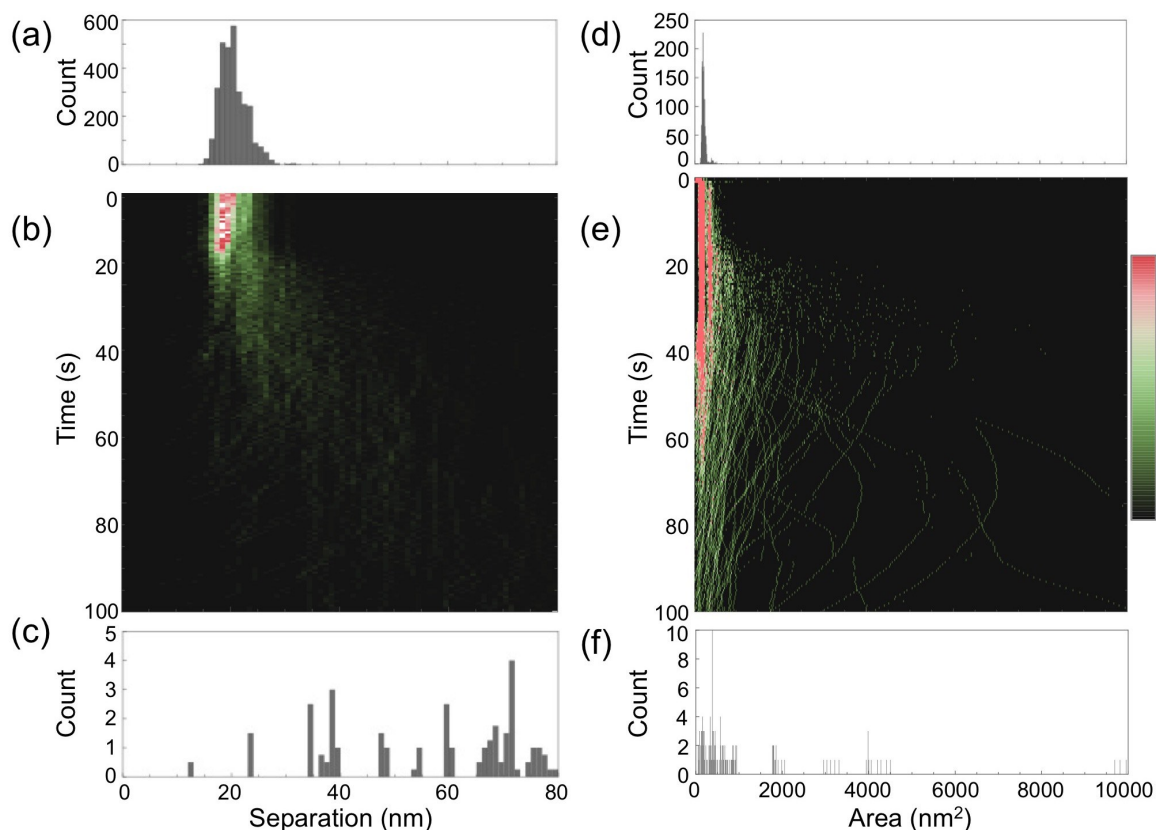


Figure S4. Advanced stages of electron damage to DNA-mediated 2D assemblies. (a) Initial histogram of center-to-center particle spacing (elapsed time $t = 10$ s in Fig. 5 (a), main text). (b) Density plot of the time evolution of the particle spacing histogram from $t = 0$ to 100 s of high-dose imaging (corresponding to image sequence in Fig. 5 (a), main text). (c) Histogram of center-to-center particle spacing at $t = 100$ s. (d) Initial histogram of projected particle area (elapsed time $t = 10$ s in Fig. 5 (a), main text). (e) Density plot of the time evolution of the histogram of projected particle area from $t = 0$ to 100 s of high-dose imaging (corresponding to image sequence in Fig. 5 (a), main text). (f) Histogram of particle area at $t = 100$ s. For electron dose information, see Table S1.

Supplementary Note 1: Calculation of the effective electron dose

The scanning and data acquisition patterns in STEM imaging, shown in Figure S5, form the basis for the calculation of the effective electron dose (or dose rate). Some of the details of the scan pattern may vary from one microscope to another, but the salient features generally remain the same.

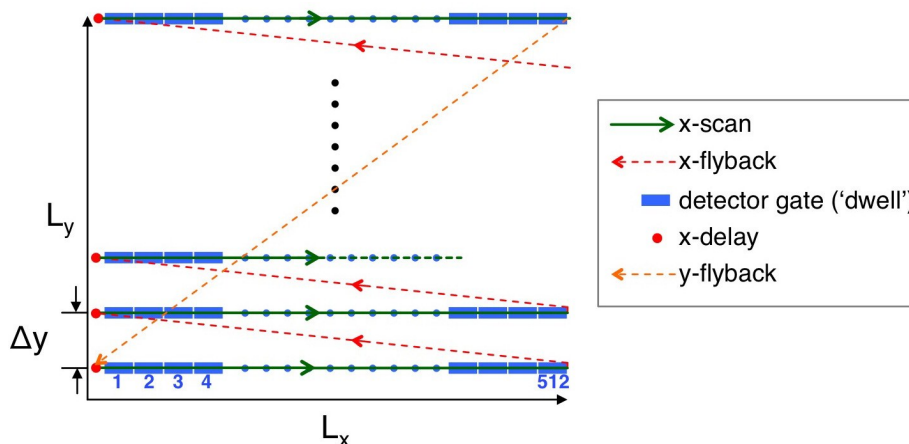


Figure S5. Scanning and data acquisition pattern in STEM. The focused probe is scanned line-by-line along the fast (x) scan direction. Each line is followed by a fast x-flyback, which positions the beam at the origin of the next fast-scan line, and by an x-delay time. After completion of the entire frame the beam is brought back to the global origin by a fast y-flyback, which initializes the next image frame. Scanning is continuous (except for the delays shown). The data acquisition, on the other hand, is performed pixel-by-pixel in discrete detector gate intervals, also known as the ‘dwell time’. Note that the term ‘dwell time’ is somewhat misleading since the beam is not stationary but maintained scanning during the gate interval. The detector signal is integrated during the ‘dwell time’ and read out as the signal associated with the corresponding image pixel.

The dose rate calculation is parameterized by the following input quantities:

- Electron beam current (I_e , measured by Faraday cup)
- Electron beam diameter (d , estimate based on microscope manufacturer data)
- Physical image size ($L_x \times L_y$, defined by the operator)
- Number of pixels per line (a) and number of lines per image (b)
- Time per frame (t_{img} , defined by the operator)

In addition, there are derived quantities (e.g., $\Delta y = L_y/(b-1)$) and quantities that are only approximately known (e.g., the x-delay and x-flyback time).

The local dose rate is determined by the time it takes the beam to scan each line. If we neglect the (unknown) x-delay and x-flyback time (small compared to the time per line, hence adding minimal additional dose), the time per line is given by the time per frame divided by the number of scan lines: $\tau = t_{img}/b$. The speed of the scanning beam is therefore $v_e = L_x/\tau$. The dose (in $e/\text{\AA}^2$) injected into any *point traversed by the scanning beam per image frame* is: $D = (I_e/e)/(v_e \times d)$, where e denotes the elementary charge. Table S1 summarizes the electron dose per image frame experienced by the points traversed by the scanning electron beam (beam size $d = 2 \text{\AA}$):

Table S1: Experimental parameters and calculated electron dose per image frame injected into the exposure track (i.e., points traversed by the scanning electron beam).

Figure No.	$L_x \times L_y$ (nm ²)	I_e (pA)	$a \times b$	t_{img} (s)	Dose/frame (e ⁻ /Å ²)
4 (a)	768.7 × 768.7	1	512 × 512	0.52	0.41
4 (b)	384 × 384	1	512 × 512	0.52	0.83
5	1090 × 1090	91	512 × 512	0.52	26.5
6	1090 × 1090	1	512 × 512	0.52	0.29
S2	2161 × 2161	27	512 × 512	0.52	3.96
S3	1540 × 1540	12	512 × 512	1.05	11.1
S4	1090 × 1090	91	512 × 512	0.52	26.5

Note that the values for the electron dose per image frame denote the dose injected into the path of the scanning beam during the x-scan (see Figure S5). Areas of the sample not scanned by the beam experience zero electron dose. This is illustrated in Figure S6. For typical low-dose imaging conditions (e.g., Fig. 6), only about 10% of the field of view is directly exposed to the scanning electron beam.

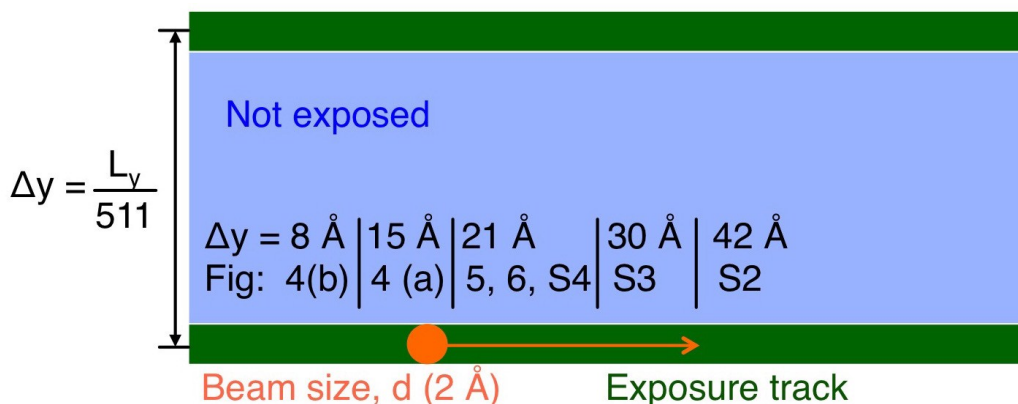


Figure S6. Pattern of beam exposure track and adjacent larger areas without exposure, i.e., with zero electron dose. The beam size of 2 Å defines the width of the exposure track. The y-increment $\Delta y = L_y/512$. Numerical values of Δy are given in the figure, along with the corresponding figure numbers in both main text and supporting information.

In time series across many image frames, scan non-idealities such as deflection coil hysteresis, fly-back distortion, and drift cause random shifts in the scan path from one image to the next. This implies that in consecutive image frames different exposure tracks are scanned, so that the dose over longer times (> 1 frame) is spread across larger areas and not simply added up along the same exposure track. This effective spreading of the electron dose supports low-dose imaging of longer time series in STEM.